Journal of Imaging Science and Technology® 56(6): 060501-1–060501-11, 2012.

Investigations of Charge Migration and Charge Trapping in Fatigued Organic Photoconductors

Zbigniew Tokarski▲, Yong-Jin Ahn, and Soo-Yong Jung
Samsung Electronics, Digital Printing Division, Suwon-City, Korea
E-mail: ztokarski@hotmail.com

Abstract. *This article presents the experimental photodischarge kinetics of electrostatically fatigued dual-layer organic photoconductors characterized by an electrophotographic incremental charging technique that reveals the differences in the photoconductor charging profiles. During normal operation, 15% of the holes that migrate to the surface after photodischarge are not neutralized by the negative surface ions. The accumulation of these lingering surface charges (charge transport material radical cations) manifests itself as defects in half-tone images, as either missing or reduced size dots or lines. In the presence of corona gases, these surface holes oxidize and reduce the energy barrier for hole injection from a positively charged surface, e.g., contact with a transfer roller. These injected holes accumulate near the charge generation layer and require twice the amount of negative charge to attain the same surface potential as that of a new organic photoconductor (OPC) drum. The damaged depth of this injection region extends to about 50 nm into the OPC surface and is easily removed by the printer's abrasion mechanisms (e.g., cleaning blade, toner, paper).* ©*2012 Society for Imaging Science and Technology.*

[DOI: 10.2352/J.ImagingSci.Technol.12.56.6.060501]

INTRODUCTION

Present-day high-volume electrophotographic printers, copiers, and image reproduction systems are expected to produce high-quality digital images throughout the intended functional life of each consumable component. Any defect or abnormality in any of these components may lessen the output quality of the digital image. There are several different types of image defect that appear as a result of organic photoconductor (OPC) fatigue (repeated charge and photodischarge), such as image blurring due to toner spreading away from well-defined lines and text, development in the white background area, and under-developed solid or half-tone regions due to smaller (or missing) dots. The fatigued OPC and the image density may recover after a prolonged period of non-usage, but the onset of the image defect reappearance requires fewer continuous prints to reproduce the defect. The occurrence and magnitude of these phenomena depend on OPC dual-layer composition, temperature and humidity, printer settings and its internal gaseous environment, and the number of imaging cycles made on the OPC imaging unit.

▲ IS&T Member.

Received Apr. 23, 2012; accepted for publication Sep. 12, 2012; published online Mar. 26, 2013.
1062-3701/12/56(6)/060501/11/$20.00

Various models are proposed to account for each of the different types of image defect produced by repeated charge and photodischarge of the OPC. Image degradation mechanisms that produce lateral motion of charges near the OPC surface include (i) the migration of surface ions due to moisture (humidity dependence) or other contaminants,[1] (ii) ohmic conduction in certain protective layers coated over the charge transport layer (CTL),[2] and (iii) the lateral motion of transit carriers that reside near the photoconductor surface after photodischarge.[3,4]

Great progress was made in minimizing or eliminating image degradation in commercial OPC drums by controlling the material formulation, fabrication process, and method used in the coating production of each OPC layer. These advances made the image degradation due to lateral charge migration a much slower process than the time required to develop the latent image. However, in fatigued photoconductors, these transit carriers can build up in a very thin region near the OPC surface after every photodischarge and form a charge double layer. Lateral motion of the charges becomes more pronounced and has been modeled and analyzed numerically.[5] The rate of lateral charge migration is dependent on the surface conductivity, latent image charge density, and its field-dependent charge mobility.[6] This phenomenon increases with repeated charge and photodischarge of the photoconductor during continuous or extended printing[7] and as the charges build up at a non-abraded OPC surface (discussed later).

In this article, we investigate the phenomena of charge accumulation near the surface of the OPC. The mode of operation for the new OPC diagnostic equipment used to study this phenomenon is fully described in the literature.[8–10] The following is a brief explanation of the principle of operation for this equipment.

In general, for a negative-type dual-layer organic photoconductor, the mobility of holes through the CTL is much higher than the mobility of electrons in the CTL. During the diagnostic procedure, the OPC voltage is incrementally increased by the deposition of small doses of negative ions (via a corotron) onto the OPC surface. The surface voltage and the electric field across the OPC will continue to increase with each negative ion deposition unless there are extractable charges trapped within any of the OPC layers. These quasi-free trapped charges (holes) reside in energy wells and are released only when the electric field across the layer is sufficiently large to overcome this restraining

force. The trapped charges that reside in the lowest-energy wells are released first and are usually found within the Charge Generation Layer (CGL) (depletion charging).[11,12] After freeing the trapped charges, the surface voltage will continue to increase incrementally with additional doses of negative ions up to the operational voltage.

Exposure of the CGL to light produces electron–hole pairs that separate in the presence of an electrical field, and each charge migrates toward its respective oppositely charged pole. The holes in the CGL will travel through the CTL (electrons toward the substrate) and neutralize the negative ions at the surface. If this neutralization is incomplete or prohibited, then these holes accumulate near the surface and form a charged double layer. In our experiment, we subsequently deposit positive charged ions to charge the OPC to a positive voltage and force any residual holes at the surface to travel through the CTL again. These holes will recombine near the CGL with electrons that are injected from the substrate. Recombination occurs either at the CGL–CTL interface, within the CGL, or at the CGL–barrier layer interface, as holes are not mobile in the barrier (anodized or undercoat) layer. The process of moving these holes through the CTL (in either direction) and quantifying the charges deposited on the OPC was carried out on a specially built electrophotographic incremental charge (EPIC) analysis device.

We present experimental results showing charge carrier accumulation near the OPC surface after extensive charge and photodischarge cycles of the OPC using a remodeled laser beam printer as the printer test-bed. The damage to the OPC surface during extensive printing (without OPC surface abrasion) changed the OPC surface from an injection barrier to a positive charge injection permeable surface. We show that the damage depth into the CTL occurs within ∼50 nm of the surface, and this damaged region is usually removed by the normal abrasive wear of the cleaning blade.

TECHNIQUES AND EQUIPMENT

A monochromatic laser printer (35 ppm), manufactured by Samsung Electronics Corporation, was reconfigured with special printer circuit boards to run under an external controller computer and with the primary charge roller, transfer roller, and laser scanning unit (LSU, $\lambda = 760$ nm) functions enabled and the paper feed, toner sensor, and pre-transfer lamp functions disabled. This printer test-bed is not equipped with an erase bar to discharge the OPC prior to recharging. Figure 1 shows a schematic of the modified toner cartridge used in this printer test-bed, with the black toner, developer roller, metering blade, and supply roller removed to create the test cartridge. The test cartridge was equipped with five Trek voltage probes around the circumference and along the axis of the OPC drum to measure and record the OPC surface potential at different locations. The probes were arranged in the test cartridge to measure the OPC surface voltage after the charge roller position (biased at −1.3 kV DC), at the developer roller position, and after the transfer roller position (biased at +1.2 kV DC and part of the

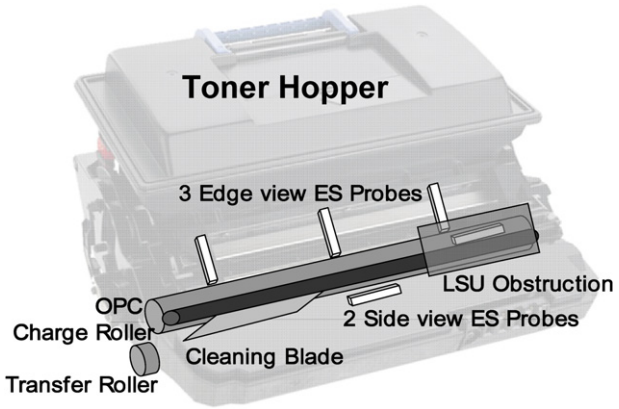

Figure 1. Schematic of a modified toner cartridge (see text for details).

printer test-bed). Three edge-view voltage probes arranged along the axis of the OPC drum at the developer roller position measured the surface potential at three different test sections. The axis of the drum was sectioned off so that the right one-third of the OPC (as viewed from the waste-bin toward the toner hopper) was charged only (LSU beam obstructed). The center one-third was charged and imaged by the laser scanning unit at 100% coverage (solid block), and the left one-third was charged, imaged (100% coverage), and abraded by a polyurethane cleaning blade (length ∼85 mm). The cleaning blade length covered only the left one-third of the OPC drum; its direction was inverted (against the OPC rotational direction) relative to this normal direction in a toner cartridge, and it was attached to the test cartridge such that the center of the blade's widest side contacted the OPC. This configuration produced OPC abrasion but did not flip the cleaning blade during extended test runs without toner.

Several identical negative-type dual-layer organic photoconductor drums (ϕ30 mm) were obtained from an OPC manufacturer in Japan and consisted of an anodized substrate (hole injection barrier), a charge generation layer (∼0.5 μm), and a charge transport layer (∼25 μm) in this layer sequence (commercial product, proprietary composition). The OPC drums were charged and photodischarged for 26,000 continuous OPC revolutions per test set. This is the equivalent to 5000 letter-sized pages printed at 100% solid coverage across the length and width of the page (excluding the 0.5 cm margins). The timing sequence in this printer test-bed was such that each full printed page required 5.2 revolutions of the OPC drum: this consisted of an imaged page (3 revolutions with LSU exposure) and the time gap between pages (2.2 revolutions without LSU exposure). A separate data-logging computer worked with the external controller computer to monitor the OPC surface potentials (all five probes) in real time and to record one page of OPC surface potentials after every 1300 OPC revolutions, i.e., surface potentials were logged at the first page and at pages 250, 500, . . . , 4750, 5000.

After 26,000 continuous revolutions (5000 pages), the fatigued OPC drum was removed from the modified test cartridge, inserted into a normal toner-filled cartridge, and a set of 50 different diagnostic image-quality test patterns

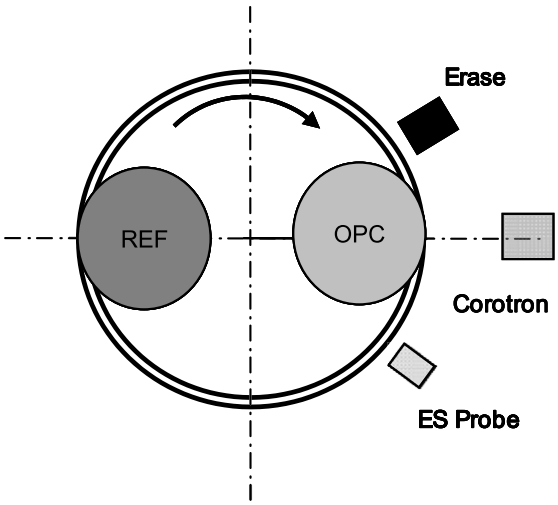

Figure 2. Electrophotographic incremental charge (EPIC) apparatus.

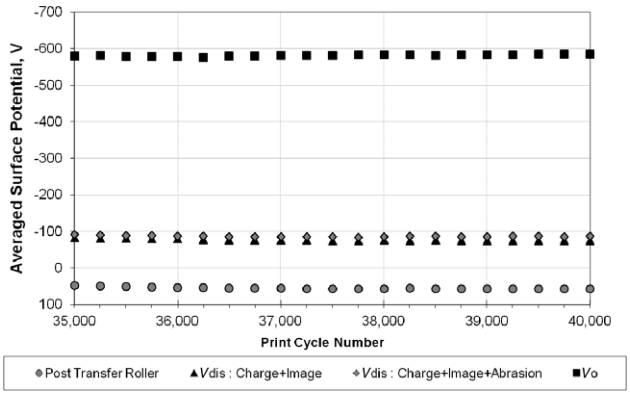

Figure 3. Surface potential for OPC-1 during the printing of the 35,000 to 40,000 page set. Data logged every 250th page and averaged in the imaged region.

were printed using a fully functional Samsung monochrome printer (model comparable to the printer test-bed). The images were evaluated for print quality, particularly the dot size, line resolution, and optical density of the solid images.

ELECTROPHOTOGRAPHIC INCREMENTAL CHARGE (EPIC) ANALYSIS

A second device evaluated the level of trapped charges within the OPC layers and operated in a similar manner as described in Refs. 8–10. Figure 2 illustrates the electrophotographic incremental charge (EPIC) diagnostic test apparatus that applied small doses of charge (small Δq) to the OPC surface until it reached the desired negative (or positive) operating potential. A rotating fixture held the OPC drum as it rotated (4 Hz) from the corotron charger location to the electrostatic probe location to measure the surface potential after each small charge deposition. At this rotational frequency, the charge leakage (dark decay rate) from a negatively charged OPC is negligible, as it is a slower process than the time frame of this experiment. In addition, electron mobility through the CTL and hole mobility through the barrier layer are extremely low and cannot discharge a positively charged OPC during our experimental timeframe.

A reference drum, set to a fixed surface potential of +200 V, was the internal reference for the electrostatic probe to ensure surface potential measurement accuracy. A National Instruments digital multimeter attached to the OPC measured the amount of charge (current versus time integral) deposited on the OPC during each rotation. The OPC was discharged using either exposure to red LED erase light ($\lambda = 780$ nm) or deposition of ion charges of opposite polarity to the existing charge on the OPC drum.

The test sequence involved incremental charging of the OPC to the desired negative operational voltage, photodischarging by LED exposure, and then charging the OPC to the desired positive operational voltage. The negative charging plus LED exposure events were repeated 1, 2, 4, 8, or 16 times before positive charging. A complete experimental run is symbolically represented in Table I, where Ni (i = 1 to 32) represents the incremental application of negative ions and X represents LED erase exposure after completion of incremental negative charging. Pj (j = 1 to 6) represents the incremental application of positive ions and N′ represents the application of negative ions after completion of incremental positive charging to neutralize the positive ions and restore the OPC to zero voltage prior to the start of the next segment. The full incremental negative charging plus LED exposure events for the fourth and fifth charging segments are not shown in Table I, for the sake of brevity. The short run duration of the seven segments of the EPIC test—in a well-vented dark enclosure at ambient temperature and humidity (20–25°C, 40–60% RH)—ensured a constant uncontaminated environment.

Table I. Electrophotographic incremental charging run sequence.

Segment	Events
1	(N1 X) P1 N′
2	(N2 X - N3 X) P2 N′
3	(N4 X - N5 X - N6 X - N7 X) P3 N′
4	(N8 X — · · · — N15 X) P4 N′
5	(N16 X — · · · — N31 X) P5 N′
6	P6 N′
7	N32

Analysis of data from this device reveals the magnitude and conditions required to (i) extract trapped charges from different energy levels in the CTL (during a Pj event), (ii) inject positive charges from the surface into the CTL (during a Pj event), and (iii) inject holes from the CGL due to thermal or electric field stimulated charge generation or due to incomplete hole–electron recombination in the CGL (during an Ni event).

EXPERIMENTAL RESULTS

OPC Charge–Photodischarge Fatigue

All of the OPC samples in this study were first fatigued in the printer test-bed (unless otherwise noted). Figure 3 illustrates

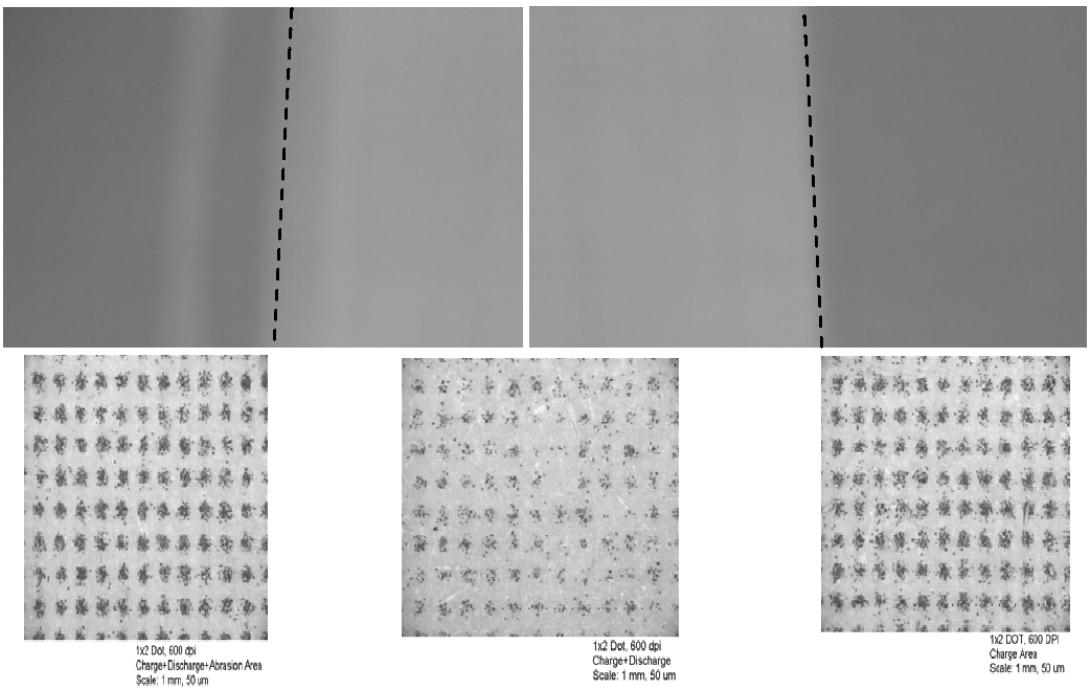

Figure 4. Photograph and micrograph of a 1-dot × 2-dot half-tone image on paper using OPC-1 (100% solid coverage for 50,000 pages). Drum treatment regions include left (charge, image, abrade via polyurethane cleaning blade), center (charge and image), and right (charged only).

the typical electrophotographic photo-induced discharge curves (PIDC) observed for an organic photoconductor drum (OPC-1) placed in the modified toner test cartridge and exercised in the printer test-bed. This OPC drum was exercised for 10 data sets of 26,000 continuous OPC revolutions per set (the equivalent of 5000 pages per data set or 50,000 pages total) and the internal electrical charge migration nature was evaluated for the OPC after every 5000-page data set on the electrophotographic incremental charge analyzer. The curves in Fig. 3 show the average surface potential of an imaged region of the OPC after every 250th page during the eighth data set (pages 35,000 to 40,000 on the printer test-bed). The charge acceptance voltage (Vo, right probe in the test cartridge) and photodischarge voltage (Vdis, center and left probes) were essentially constant for the 5000 pages in Fig. 3 and over the entire 10 data sets (50,000-page test). Based on these results alone, one would predict that no changes occurred to the OPC drum's electronic structure or chemical composition. In addition, the OPC voltage was constant at about +60 V after direct contact to the transfer roller (transfer probe on test cartridge). Indirect contact exists during normal printing when paper is present between the OPC and transfer roller. Any change in the slope of these curves would indicate that charges were building up within the OPC with each charge and photodischarge cycle (increase in residual surface voltage, Vdis) or that the OPC could not maintain a constant charge acceptance voltage (Vo decrease due to dark decay).

The OPC after the tenth data set was placed in a normal toner cartridge for printing with toner and paper. A set of diagnostic image-quality test patterns revealed differences in the half-tone image density for the three test sections across the drum. Figure 4 shows a photograph (top) and micrograph (bottom) of a 1-dot × 2-dot half-tone pattern after transferring the toned image to paper from this OPC drum. The center of the photograph represents the area of the OPC that was repeatedly charged and discharged for 50,000 pages (no cleaning blade present to abrade the OPC), while the left side of the photograph represents a section of the drum that was charged, discharged, and abraded by a cleaning blade (see Fig. 1). The lighter center image was due to weak single-dot intensity and missing dots. Removal of the damaged surface by cleaning blade abrasion on a real-time basis (left side) or after the buildup of subsurface charges (discussed later) significantly improved the quality of these images. The combination of charge and photodischarge (center) decreased the image quality (smaller dot size) more rapidly than just by charging of the OPC surface alone (right side of Fig. 4; no exposure and no cleaning blade). Deposition of negative ions and very reactive neutral molecules (e.g., ozone, NOx, etc.) during charging is expected to oxidize the surface of the OPC, and this would be sufficient to significantly alter the image quality.[13,14] It is evident from these results that the charging process alone (no exposure and no abrasion) was not sufficient to deteriorate the image (decrease the single-dot intensities or delete dots). The combination of negative charging and LSU light exposure, where holes were generated within the CGL and then migrated through the CTL, significantly increased the image degradation rate over just negative charging alone.

To help identify the role that these holes, surface ions, and reactive neutral molecules play in producing the image defects, a method was devised to determine the hole quantity and final location within the OPC. Our

conventional understanding is that the negative surface ions and charge transport material (CTM) radical cations interact at the CTL–air interface in a manner that "neutralizes" both species. If this type of interaction is prohibited, then the holes remain within the CTL and are neutralized by another (slower) mechanism—that is, by a mechanism that invokes the lateral motion of holes near the surface but still within the CTL.

Incremental charging baseline

The characteristic curves generated by incrementally charging the OPC surface provided information regarding the charge carrier injection and extraction processes that takes place within the dual-layer photoconductor. Figure 5 illustrates the set of baseline curves that were generated by the EPIC analysis instrument for a new unfatigued reference photoconductor drum, OPC-2. Fig. 5(a) shows the curve of the surface potential versus EPIC fixture revolution number for the 32 negative and 6 positive charge sequences used in all of the EPIC experimental runs. An additional curve of the cumulative charge deposited on the OPC versus EPIC revolution number was also generated (not shown). In Fig. 5(a), curve N1 traces out the initial increase in negative surface voltage and the exposure to red LED light ($\lambda = 780$ nm) to photodischarge the photoconductor. Incremental positive charging (curve P1) and subsequent deposition of negative ions brought the surface potential back to zero for the start of the next charging segment (Segment 1, $(\mathrm{N1} \cdot X) \cdot \mathrm{P1} \cdot \mathrm{N}'$ events).

Fig. 5(b) is obtained by replotting the data (voltage and absolute surface charge density $|Q|$[uC/cm^2] versus EPIC rotation) as the sum of the incremental charges deposited on a unit area of the OPC surface on the ordinate axis versus the measured surface voltage on the abscissa axis, and each curve was forced to go through the figure origin. The S-shaped (sigmoidal) charge–voltage characteristic curves in Fig. 5(b) have a small initial linear growth region from 0 V to +75 V (capacitive charging: $\mathrm{d}Q = C * \mathrm{d}V$ with charge Q, capacitance C, and voltage V); a prominent logarithmic growth (depletion voltage range) region from +75 to +100 V; and then a transition to a voltage-dependent capacitance charging region ($\mathrm{d}Q = C(V) * \mathrm{d}V$) that was dependent on the segment number of the positive charging event (P1 to P6). The voltage range in the logarithmic region represents current flow through the photoconductor due to the detrapping of quasi-free holes near the surface of the OPC, their migration through the CTL toward the CGL, and subsequent recombination with electrons injected from the substrate (see Ref. 9). The magnitude of the sigmoidal region increased as the number of repetitive negative charge plus LED exposure events increased prior to positive charging (curves P1–P5). Subsequent positive recharging of curve P5 (after negative charge deposition to attain zero voltage) produced a positive charge–voltage curve (curve P6) without a sigmoidal region and with a nearly constant slope above +150 V. All of the repetitive negative charging events (N2–N32) had similar overlapping charge–voltage curves as the initial negative charging segment, curve N1, and are not displayed in the graphs

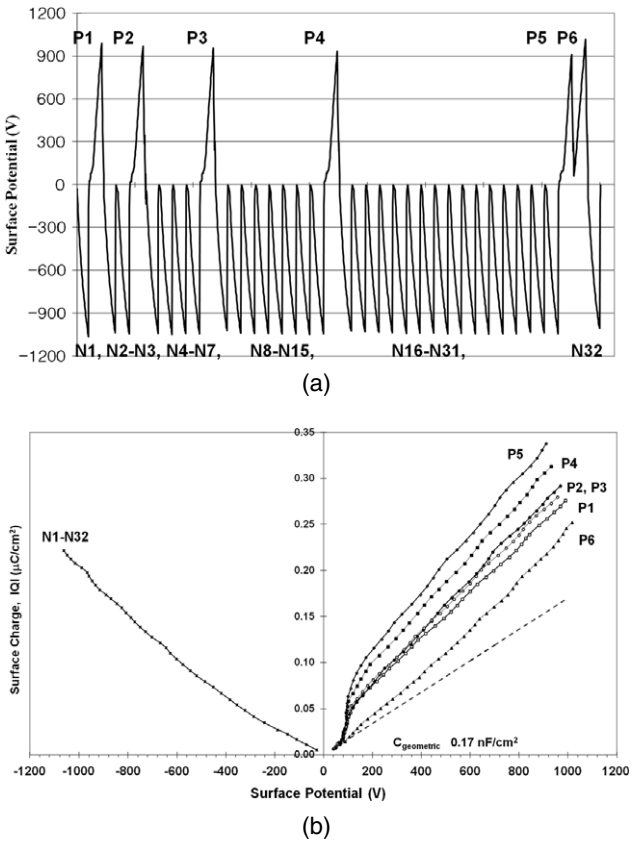

Figure 5. Charge–voltage characteristics of negative and positive incremental charging of OPC-2: (a) the 38-segment sequence (6 positive and 32 negative) and (b) charge–voltage characteristics. Curve N*i*: incremental negative charging segment; Curves P1 to P5: incremental positive charging after 1, 2, 4, 8, or 16 cycles of negative charging and discharge to zero by exposure to red light, respectively; and Curve P6: incremental positive recharging after discharging the photoconductor in curve P5 to zero voltage.

The effective capacitance (C_{eff}) (the mathematical derivative of a curve at its corresponding surface potential) for all of the positive curves tends toward 0.17 nF/cm^2 at low surface potentials (negative curves tend toward 0.12 nF/cm^2). This represents the apparent geometric capacitance of the photoconductor (Fig. 5(b); dashed line going through the origin) and assumes no charge leakage. Linear extrapolation of the steep portion of the curve in Fig. 5(b) to zero surface charge intersected the abscissa axis at +72 V, the onset voltage for logarithm growth.

Surface oxidation

Oxidation of the CTM within the CTL is a well-known contributor to OPC damage and fatigue.[14] We investigated three sets of OPC samples to ascertain the difference in damage due to three increasing corona gas-rich environments and tested a fourth OPC in a similar environment but with more charge and photodischarge cycles.

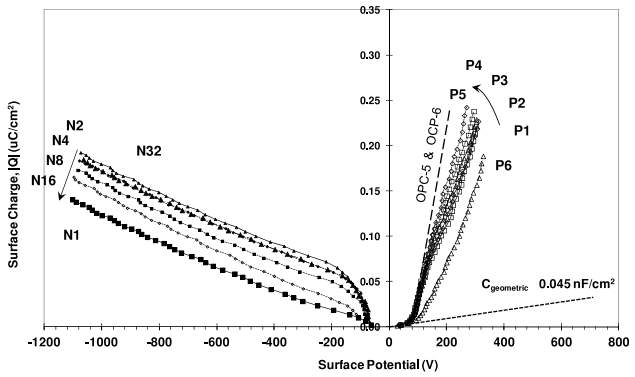

Figure 6. Charge–voltage characteristics of incremental negative and positive charging of OPC-4 after 5000 pages. The curves were produced by plotting the absolute value of the surface charge |Q| against the corresponding positive or negative surface potential.

Three OPC drums were exercised sequentially for 26,000 continuous revolutions each (5000 pages) in the printer test-bed to expose each subsequent OPC drum (OPC-3 → OPC-4 → OPC-5) to an increasing level of ozone, NOx, and other gaseous by-products under normal printer test-bed ventilation conditions. As a comparison, a fourth OPC drum (OPC-6) was exercised for twice as many revolutions (10,000 pages) after venting the printer test-bed overnight to give an final corona gas level falling somewhere between that experienced by OPC-4 and OPC-5. The non-abraded center portion of each OPC drum (no cleaning blade) was studied in detail. The PIDC electrophotographic cycling behavior for all of the drums looked identical to Fig. 3, but the EPIC charge–voltage characteristics revealed differences in the hole migration and neutralization mechanism for each drum.

The charge–voltage characteristic curves for the fatigued drum OPC-3 had roughly the same general shape as those for the unfatigued drum OPC-2 (Fig. 5(b)). The main difference was that OPC-3 required 25% less surface charge to reach the same negative or positive surface potentials as in OPC-2 and that the positive curves (P1–P6) in OPC-3 were slightly steeper and grouped closer to the P5 curve.

Figure 6 illustrates the charge–voltage characteristic curves for OPC-4. Several differences are quite notable and are due solely to the internal printer test-bed environment. First, the positive charge–voltage characteristic curves for OPC-4 exhibited a steeper slope after the logarithmic growth portion and were slightly separated from each other above +120 V. The maximum surface potential for curve P5 was +270 V (charge deposition of 0.24 $\mu C/cm^2$) and the corresponding value for curve P6 was +327 V (charge deposition of 0.19 $\mu C/cm^2$).

Second, the negative charge curves that followed the positive charging segment (N2, N4, N8, N16, and N32) displayed an S-shaped charge–voltage characteristic from −70 to −110 V, but this region did not have the same type of logarithmic rise as seen in the positive charged curves. The magnitude of this negative S-shaped region decreased as the number of repetitive negative charge plus LED exposure events prior to positive changing increased. That is, the negative charge acceptance for curve N16, which followed the "eight negative charge plus LED exposure events and one positive charge event" sequence displayed the lowest magnitude, and was closest to curve N1. Curve N2, which followed the "single negative charge plus LED exposure event and one positive charge event" sequence, displayed the highest magnitude and was closest to curve N32. Curve N32 is the negative charge segment that followed the two consecutive positive recharging segments (P5–P6) near the end of the EPIC experimental run.

All of the subsequent negative recharge curves (N3, N5-N7, N9-N15, and N17-N31) exhibited charge–voltage characteristics that overlapped curve N1 below −130 V (a very small S-shaped curve exists for N1 at −60 to −130 V). These additional 26 negative curves indicated that the holes were completely depleted from the CGL region during the first negative charging event of each segment, and they were omitted from the figures for clarity.

Finally, the shape of the negative charge–voltage curves for OPC-5 and OPC-6 were very similar to those from OPC-4. The positive charge–voltage curves (P1–P6) for OPC-5 and OPC-6 were identical, and they overlapped each other at the position represented as the dashed line in Fig. 6. The dashed line overlapped the steep rise portion of the curves for OPC-4, and the slope of these curves remained steep even above +120 V, i.e., the end of the logarithmic section for OPC-4. It is worthwhile noting that the positive and negative charge–voltage characteristic curves for OPC-5 are identical to those obtained for OPC-1 in the exposed but non-abraded region.

The following experiments addressed whether this change was permanent or if the charge–voltage characteristics recovered after some period of non-usage (dark storage at 25°C). Figure 7 shows the charge–voltage characteristics for OPC-4 and OPC-5 after a three-day storage period in the dark and without any additional cycling on the printer test-bed. The shape of the charge–voltage characteristic curves for OPC-3 did not significantly change after the three-day recovery period, while the curves for OPC-6 were identical to those from OPC-5. The shape of the positive charging curves for OPC-4 after the three-day recovery period approached the shape of the curves for OPC-3 immediately after the 26,000 revolutions. During this same period, the shape of the positive curves for OPC-5 (and OPC-6) was similar to the charge–voltage curves of OPC-4 (see Fig. 6) taken immediately after the 26,000 revolutions.

In Fig. 7(a), the charge–voltage characteristic behavior for the positive charge event displayed a linear region below +65 V, but the slope of the curves above +135 V increased with each succeeding positive charging curve (P1–P5). Although curves P1, P2, and P3 for OPC-4 looked similar to those of OPC-3, the slope of the P4 and P5 curves increased at a faster rate (steeper slope) than their counterparts in OPC-3. This indicated an incomplete recovery and that the situation can rapidly revert to the degraded condition as it was immediately after cycling for 5000 pages.

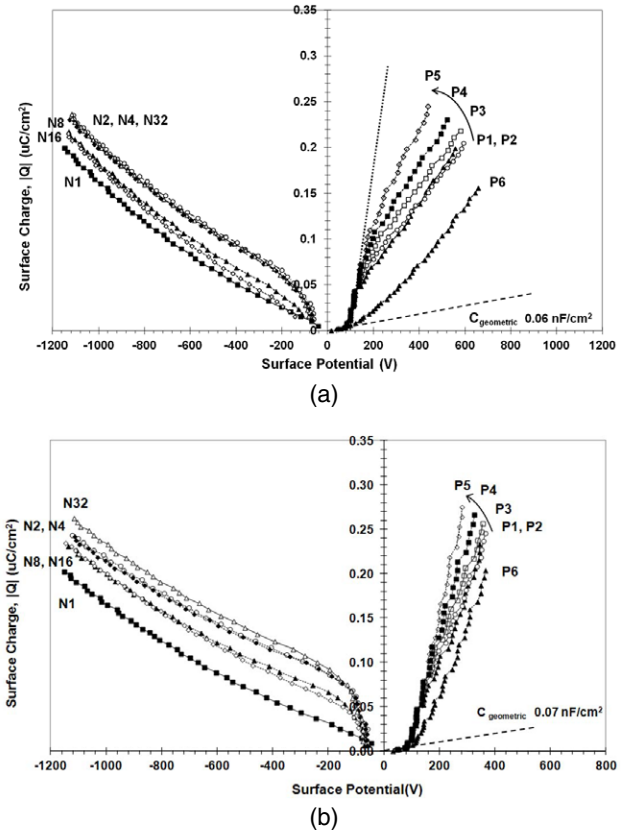

Figure 7. Charge–voltage characteristics of incremental negative and positive charging for OPC-4 (a) and OPC-5 (b) after recovering 3 days in the dark.

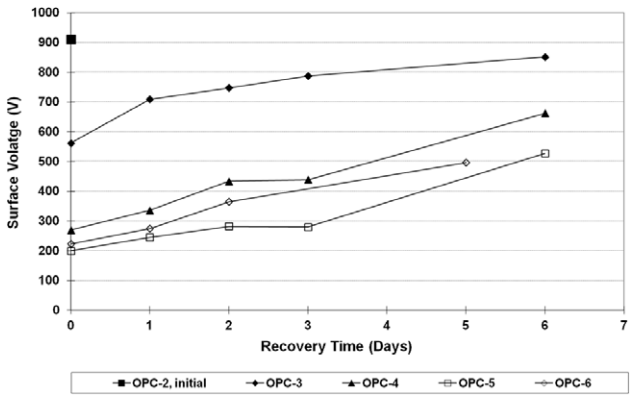

Figure 8. Maximum surface voltage for P5 incremental positive charging segment as a function of recovery period for OPC-3, OPC-4, OPC-5, and OPC-6.

Consecutive positive charging (P5→P6) in OPC-4 revealed that the preceding 31 negative and 5 positive charging events caused the OPC to remain as a highly fatigued drum. When a line was extended from the logarithmic region toward higher deposited charge (dotted line in Fig. 7(a)), it became obvious that the inflection point (transition from the logarithmic to the voltage-dependent charging region) increased in surface potential, and the slope for each succeeding positive curve became steeper. Curve P6 followed the positive recharging of curve P5, and its position on the graph occurred between the initial fatigued P6 curves of OPC-3 and OPC-4.

Fig. 7(b) shows that the slopes of the positive curves for OPC-5 decreased in magnitude as compared to their original overlapping curves. The extent of recovery was less than that of the OPC-4 because the initial damage to OPC-5 was presumably more severe. As a result, the positive charging curves still lacked the S-shaped response observed for OPC-4. This indicated that a portion of the deposited surface charges went toward increasing the surface potential, while the other portion produced a current through the CTL toward the CGL.

The curves from the first negative charge plus LED exposure events that immediately followed the positive charging curves still maintained the S-shaped characteristic of the fatigued drums. The main difference between the negative curves for OPC-4 and OPC-5 was the quantity of negative charges that was required to attain a certain surface potential. As an example, the deposition of 0.1 $\mu C/cm^2$ charge density produced an N32 curve surface potential of -450 V for OPC-4 ($C_{\text{eff}} = 0.22$ nF/cm^2) and only -240 V for OPC-5 ($C_{\text{eff}} = 0.42$ nF/cm^2).

It is clear from Fig. 7 that the charge–voltage characteristics of the lightly damaged OPCs began to recover during a period of non-use. Figure 8 illustrates the recovery process for the four fatigued OPC drums by plotting the maximum surface potential achieved for curve P5 over a six-day recovery period. The recovery curve for OPC-6 occurred between those of OPC-4 and OPC-5, indicating that the environment experienced by OPC-6 was probably intermediate to the internal printer test-bed environment of OPC-4 and OPC-5. These curves show that the recovery process is slow and incomplete after six days, even for the least stressed OPC-3, as none of these curves reached the initial +900 V value. In addition, drum OPC-1 that was heavily damaged (@ 20K pages, not shown) did not recover with rest time; the P1–P6 slopes were constant and similar to those observed for OPC-5 in Fig. 7(b).

The rate of recovery of these P5 curves, without any additional external assistance to hasten recovery, is too slow a mechanism to rely on in commercial printers. As a comparison, photoconductors taken from normal toner cartridges after printing 5000 pages (cartridge containing a cleaning blade and transferring the toned image to paper) displayed P5 curves that were similar to those observed for new OPCs (e.g., OPC-2). The main difference is that the OPC from the normal toner cartridge experienced a substantial amount of abrasive wear due to the cleaning blade. The degree and depth of damage to the OPC-6 surface was determined through a gradual abrasive removal of the surface of the charge transport layer. Drum OPC-6 was placed in a normal toner cartridge (toner, cleaning blade, etc.), and the printer test-bed that was set up to run an abrasion pattern that consisted of printing one 2 mm line cross the page after every 10 blank pages to prevent the cleaning blade from flipping over during a 50-page abrasion run (no paper).

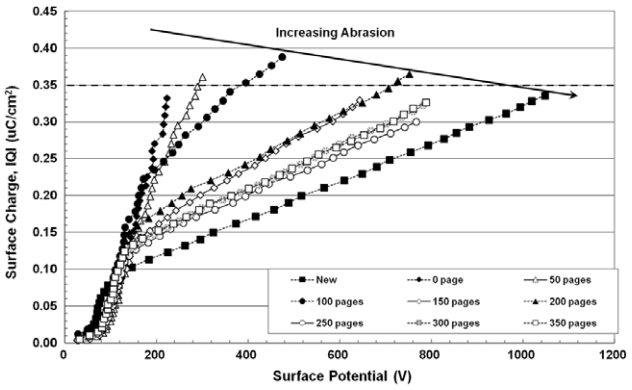

Figure 9. Charge–voltage characteristics for the P5 curves as a function of surface abrasion (pages printed) for OPC-6.

Figure 9 shows the complete set of P5 curves obtained for OPC-6 as a function of successive 50-page abrasion runs using the abrasion pattern described above. If we consider the recovery target to be +900 V at a surface charge density of 0.35 μC/cm^2 then, after extrapolating a few of the P5 curves, approximately 250–350 printed pages were required to abrade the surface enough to restore the P5 surface potential back to about +900 V. The 350 printed pages corresponded to a damaged depth of about 50 nm into the CTL surface. This depth was determined based on a experimentally observed wear rate of 1.4 μm per 10,000 prints using this abrasion pattern on the printer test-bed.

DISCUSSION

Charge migration

Figure 10 represents the sequence of actions that take place during EPIC analysis and highlights the negative charging plus LED exposure, positive charging, and the first subsequent negative charging events. The process of OPC discharge is straightforward: negative charging plus LED exposure (a), hole–electron pair generation (b), charge separation (c), hole injection (d), hole migration toward the CTL–air interface (e), electron injection into the barrier layer (d'), and electron migration toward the substrate. Holes at the CTL–air interface either are neutralized (f) by the surface negative ions (electrons are neutralized by the ground plane) or linger and accumulate as CTM radical cations near the surface (g) to form a thin charge double layer (c.d.l.).

The middle portion of Fig. 10, labeled Positive Charge, illustrates the sequence of events that occur when the polarity of the OPC is reversed. Holes in the charge double layer (g) or holes injected from the surface (k) (and electrons injected from the substrate) are forced to migrate (h) toward the opposite pole. The holes and electrons either recombine at a CGL interface (i), within the CGL (j), or become immobilized at their respective non-conductive interface. Hole and electron displacement (distance traveled) within the thin CGL is insignificant and has no marked influence on the voltage or linearity of the charge–voltage characteristic curves. That is, the change in surface voltage is 50 times greater for holes traveling through the CTL (25 μm) than for

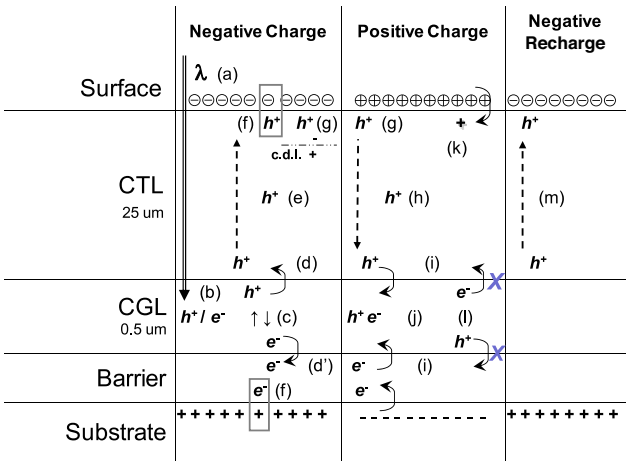

Figure 10. Charge migration within the OPC after deposition of negative or positive surface ions.

holes traveling only through the CGL (0.5 μm) toward the barrier layer (substrate).

The right side portion of Fig. 10, labeled Negative Re-Charge, illustrates the first negative charging event after positive charging but before LED exposure. Any residual holes that lingered within the CGL region or were generated in the CGL due to high local electric fields were able to migrate through the CTL (m) as the OPC was incrementally negative charged (depletion charging).

New OPC

In new OPC drums (e.g., OPC-2), the dark decay rate for positively charged photoconductors is a very slow process, indicating that positive charge injection ((k) in Fig. 10) from the surface does not occur under normal situations. The OPC charged as an ideal positive capacitor to a surface potential of about +75 V (electric field of 3 V = μm). The surface potential remained nearly constant, with the addition of 10^{11} cm^{-2} charge density, until the electric field reached 4 V = μm. In this electric field range, a significant number of quasi-free charges were released from their trapping energy wells near the free surface, drifted toward the CGL, and recombined with electrons that were injected from the substrate. This indicated that even new OPC samples accumulated unneutralized charges at the free surface following photodischarge. In high quantities, these charges are subject to lateral motion and image distortion.

The increasing charge density with each successive positive segment suggests that each negative charge and photodischarge event contributed additional holes to the charge double layer. The ratio of the quantity of quasi-free charges at the free surface to the charge density required to reach the negative operating potential is approximately 1:6.5. This means that about 15% of the holes that were generated after any photodischarged event lingered as CTM radical cations near the free surface. Any further buildup of these quasi-free charges beyond the 10^{11} cm^{-2} charge density would likely increase the leakage current away from these trap sites because of the increased localized electric fields at the surface charge double layer.

After these holes were freed, the slope of the positive charging curves (> +100 V) decreased but was not exactly parallel to the apparent geometric capacitance, $C_{\text{Geometric}}$, curve. Each positive charging event trapped more holes in successively deeper energy wells (chemical or physical barriers) in the CTL and required higher electric fields to release them. Recharging of the OPC (P6) showed that most of the lingering holes were removed from the surface by the previous positive charging event (P5). Curve P6 increased at low surface potentials along the apparent geometric capacitance curve (0.17 nF/cm^2 for new OPC versus 0.05 nF/cm^2 for fatigued OPC). The thickness of the OPC layers remained constant, so the ''true'' geometric capacitance is constant. However, OPC fatigue changed the apparent geometric capacitance of each OPC drum.

Changing the surface potential from positive to negative produced a linear charge–voltage characteristic curve for all of the negative incremental charging events (N1–N32). This indicated that all of the holes from the positive charging process recombined with the injected electrons upon reaching the CGL and that no additional holes were available to migrate toward the surface during the negative charging process.

These observations contrast with the S-shaped curves observed during the first negative charge process (N2, N4, N8, N16) of fatigued OPCs, indicating that some of the holes (extracted and injected charges) in the fatigued OPCs did not recombine with injected electrons and were completely removed from the CGL during the first negative charging process.

Fatigued OPC

The extent of fatigue varied with exposure to the oxidizing environment within the printer. OPC-3 showed differences in the charge–voltage characteristic curves relative to OPC-2 that indicated that OPC-3 was stressed but not to the level where additional charges were injected from the CTL–air interface. In the absence of charge injection, the slope of the charge–voltage characteristic curves was within a small multiple of the $C_{\text{Geometric}}$ curve. The other fatigued OPC drums behaved differently when the drum was positively charged.

The actual mechanism for the steep positive slope region of the positive charge–voltage characteristic curves is quite complex and involves charge extraction and injection. Charge extraction of the trapped positive charges that accumulated in the charge double layer was observed for new, partially fatigued, and recovering OPCs. The increasing slope after the steep rise portion of the curves indicated that more charges were trapped in and released from deeper-energy wells than the preceding positive curve. Alternatively, the steep rise region in fully fatigued OPCs continued to increase with additional charge deposition, and this is indicative of current flow through the CTL. In previous experiments, a second steep rise region in the charge–voltage curve was observed for new OPCs beyond the voltage-dependent capacitance region where high charge leakage preceded dielectric breakdown.[10] The extraction of accumulated charges in the low-voltage region (about +180 V) for fully fatigued OPC-5 and OPC-6 was expected to deplete the lower-energy sites of trapped charges. The data show that, after the P5 positive charging event, the P6 curve retraced the previous positive curve instead of forming a new S-shaped curve. This could only occur if other trapped holes immediately filled the low-energy trap sites from the higher-energy trap sites. The other evidence implicating charge injection in these OPCs includes the deposition of more positive charges (0.22 μC/cm^2) than negative charges (0.13 μC/cm^2) (holes generated during photodischarge) in the first charging sequence.

The first negative charging event that followed positive charging for these fatigued OPCs deviated from the capacitive charging curve observed for OPC-2 (and OPC-3). These fatigued OPCs exhibited a negative nonlinear region from −60 to −130 V due to hole extraction from the CGL before resuming a linear increase in voltage with negative charge deposition that ran parallel to the N1 curve. The subsequent negative charge and photodischarge curves all produced charge–voltage characteristic curves that were identical to the N1 curve. This showed that the hole reservoir that was localized in the CGL was already depleted after the first negative charging event.

One issue that needs to be addressed is the origin of the holes observed in the first negative charging curves. Potential mechanisms span from new hole formation due to high electric field stimulated charge generation in the CGL to the failure to neutralize the injected holes in the CGL. During positive charging, holes that were trapped near the surface and the additional holes that were injected from the surface migrated toward the substrate. Some of these holes recombined with injected electrons in the CGL, while those that were not neutralized became immobilized at the CGL–barrier interface. At the same time, electrons were injected into the CGL from the substrate, but in quantities that were insufficient to recombine with all of the injected holes. The electric field across the barrier layer was reduced by 1/3 because the fatigued OPC was only able to charge to a +300 V surface potential. This weak electric field may be below the electron injection energy threshold for this anodized substrate. The first negative charging event completely depletes this hole reservoir, as evident from the subsequent negative charging events, i.e., they all overlapped N1.

The next issue is the magnitude of the first negative charging events (N2, N4, N8, N16, N32) with respect to the number of negative charging curves prior to positive charging. All of the negative charging curves in the figures were bracketed by curves N1 and N32, as summarized in Table II. Curve N1 is the baseline curve representing no available holes for extraction from the CGL, while curve N32 represents the maximum quantity of extracted holes. The order of the observed negative curves and the magnitude of charge extraction is clearly related to the number of negative charge plus LED exposure events prior to the

Table II. First negative charge–voltage curves.

Curve	Prior events	Surface trapping	CGL hole extraction
N32	0*(NX) P6	Most → Least	Least → Most
N2	1*(NX) P1		
N4	2*(NX) P2		
N8	4*(NX) P3		
N16	8*(NX) P4		
N32′	16*(NX) P5 (assumed)		
N1	Pre-P1: *equivalent to* $(NX)_{\infty}$, *No P*		

positive charging event. Event N32′ is inserted into Table II for continuity to show where this curve would appear in the graphs if the P6 positive charging event was omitted.

A mechanism involving the magnitude and location of injected holes and electrons will have to be proposed to explain the increasing magnitude of these S-shaped curves. In new OPCs, detrapped CTM radical cations from the charged double layer recombine with an equal number of injected electrons, with each consecutive negative charging event contributing to the quantity of trapped holes ($16 * (NX) > 1 * (NX)$).

In fatigued OPCs, charge injection from the surface contributes to the number of holes reaching the CGL and lowers the maximum achievable positive surface potential. The maximum positive surface potential also decreased as the number of negative charging events increased (P1–P5) up to the point where all of the positive curves overlapped for severely fatigued OPC-5 and OPC-6. This is the most extreme situation where the amount of surface charges and injected charges were similar for each positive charging curve. Any proposed mechanism has to account for the number of negative charging events prior to positive charging, since all of the curves from the positive charging events overlap. From Table II, we can deduce that the 1*(NX)P1 prior event contributed the least number of trapped charges and, from the graphs, the highest quantity of extracted (unneutralized) holes from the CGL (N2), while the 8*(NX)P4 prior event contributed the most trapped charges and the lowest quantity of extracted holes (N16).

The final issue is the cause for positive charge injection from the surface. This is related to the condition of the CTM near the free surface. CTMs used in modern photoconductors are selected to have little or no permanent damage upon exposure to light only. CTMs in the process of charging are exposed to oxidizing surface gases (ozone, NOx) that can change the CTM radical cation into a CTM form that facilitates charge injection.[14] From Fig. 4, we see that fatigue is greater for the oxidized CTM radial cation (center, charge + discharge) than for the oxidized CTM (right, charge only). In the situation where lingering holes exist in the charged double layer, these CTM radical cations are oxidized into a form that promotes charge injection from the surface. It is unknown from our experiments if the oxidized structures are different or if the structures are identical and that the oxidation rate is faster for the CTM radical cations.

Half-tone images

As expected, the half-tone printed images were lightest in density for the drum section where holes accumulated at the CTL surface. The prerequisite for this degradation process to occur is that the OPC surface must be damaged by repeated charged and photodischarged in the presence of an oxidizing internal printer environment. Our results have shown that printing the equivalent of 5000 pages in a contaminated printer environment produced sufficient damage to the surface of OPC-5. Any printer system without a cleaning blade must be well vented to avoid the type of OPC damage described in this investigation.

Conventional PIDC electrophotographic testing methods that only measure the net OPC surface potentials will not detect this type of damage. The OPC surface potential after image transfer (transfer roller station in Fig. 3) was about +60 V. The electric field at this positive surface potential may not be sufficient to release the lingering trapped charges at the OPC surface. These charges would still be free to move laterally along the OPC surface (causing image degradation) and subject to oxidative damage. It would be interesting to see if periodic purging of these lingering surface charges would improve image quality and decrease OPC fatigue in the absence of a cleaning blade.

CONCLUSION

A new incremental charging test method was proposed to quantify the accumulation of trapped charge carriers near the OPC surface after a typical charge and photodischarge event and to characterize the injection of positive charges from a hole permeable surface of fatigued photoconductors. Approximately 15% of the holes that migrate to the surface after a typical OPC photodischarge event are not neutralized by the negative surface ions. The accumulation of these trapped CTM radical cations at the surface of the photoconductor is not detectable using standard PIDC electrophotographic evaluation methods, such as an increase in the discharge voltage, due to the very close proximity of the holes to the surface. When the surface potential is reversed, these charges are able to migrate across the entire CTL length (25 μm) and produce an observable voltage so that we could quantify the effect and determine the location of these trapped surface charges. The effect of these lingering surface holes created a charged double layer, and manifests itself as defects in half-tone images, as either missing or reduced size dots or lines.

In the presence of corona gases, and with insufficient OPC surface abrasion, the repeated negative charge and photodischarge of the OPC oxidizes these surface CTM radical cations and reduces the energy barrier for hole injection from a positively charged surface, e.g., after contact with a positive transfer roller.

An electric field of $(+)3 - 4$ V $=$ μm is required to release the quasi-trapped holes from the surface, and even higher electric fields are required to release the holes from deeper trapped sites or to injection holes from the damaged surface. The injected charges accumulated in the CGL and required twice the quantity of negative charges to attain the same surface potential as that of a new OPC drum.

The damaged depth of this charge injection region extends to about 50 nm into the OPC surface after printing the equivalent of 10,000 pages. An abrasion mechanism (e.g., cleaning blade, toner, paper) normally removes this damaged surface. Printer and developer unit design play a key role in producing high-quality half-tone images. Adequate venting and a periodic positive charging to clear the surface of lingering holes should reduce the required cleaning blade pressure on the OPC and prolong OPC thickness and operational life.

ACKNOWLEDGMENTS

One of the authors (Z. Tokarski) would like to acknowledge helpful discussions with Prof. Jonas Sidaravicius from the Vilnius Gediminas Technical University, Lithuania and Prof. Valentas Gaidelis from Vilnius University, Lithuania.

REFERENCES

[1] E. J. Yarmchuk and G. E. Keefe, "High-resolution surface charge measurements on an organic photoconductor," J. Appl. Phys. **66**, 5435 (1989); E. J. Yarmchuk and G. E. Keefe, "Motion of surface charge on layered organic photoconductor," J. Imaging Sci. Technol. **35**, 232 (1991).

[2] D. S. Weiss, J. R. Cowdery, W. T. Ferrar, and R. H. Young, "Analysis of electrostatic latent image blurring caused by photoconductor surface treatments," J. Imaging Sci. Technol. **40**, 322 (1996).

[3] J. Yi and R. B. Wells, PC surface charge density from a vertically Gaussian, laterally exposure-based volume charge distribution in the CGL, *Proc. IS&T's NIP19: Int'l Conf. Digital Printing Technol.* (IS&T, Springfield, VA, 2003) pp. 91–96.

[4] Y. Watanabe, H. Kawamoto, H. Shoji, H. Suzuki, and Y. Kishi, "A numerical study of high resolution latent image formation by laser beam exposure," J. Imaging Sci. Technol. **45**, 579–586 (2001).

[5] J. Yi and R. B. Wells, "Numerical simulation of the lateral conductivity of a photoconductor surface," J. Imaging Sci. Technol. **48**, 294 (2004).

[6] I. Chen, J. Mort, M. A. Machonkin, and J. R. Larson, "Degradation of electrographic images due to surface lateral conduction," J. Imaging Sci. Technol. **40**, 431 (1996).

[7] Z. Tokarski and Y. J. Ahn, "Charging characteristics of fatigued photoconductors," J. Imag. Soc. Jpn **47**, 494–500 (2008) [English]; Z. Tokarski and Y. J. Ahn, "Charging characteristics of fatigued photoconductors," *Proc. ISJ's Pan-Pacific Imaging Conf. '08, Tokyo* (ISJ, Tokyo, Japan, 2008) pp. 112–115.

[8] P. J. Žilinskas, E. Montrimas, and T. Lozovski, "Measuring the parameters of dielectric layers by periodically charging the surface," Technical Phys. **51**, 1372–1378 (2006).

[9] Z. Tokarski, Y. J. Ahn, V. Gaidelis, R. Maldzius, T. Lozovski, and J. Sidaravicius, Incremental charging method to elucidate the role of (+) trapped charges near the OPC surface in electrostatic image defect formation, *Proc. IS&T's NIP23: Int'l Conf. on Digital Printing Technol. and Digital Fabrication 2007* (IS&T, Springfield VA, 2007) pp. 643–648.

[10] E. Montrimas, T. Lozovski, J. Sidaravicius, and Z. Tokarski, "Charging transients of organic electrophotographic photoconductors," J. Imaging Sci. Technol. **49**, 326 (2005).

[11] S. Jeyadev and D. M. Pai, Depletion charging in photoconductors. *Proc. IS&T's NIP11: Int'l. Congress on Advances in Non-Impact Technol.* (IS&T, Springfield, VA, 1995) pp. 141–146.

[12] C.-W. Lin, T. Nozaki, and Y. Hoshino, Analysis of Traps in Photosensitive Materials from the Dependence of Corona Charging Characteristics on Exposure, *Proc. IS&T's NIP13: Int'l Conf. on Digital Printing Technol.* (IS&T, Springfield, VA, 1997) pp. 270–273.

[13] K. Nauka, S. Chang, and H. T. Ng, "Surface modification of an organic photoconductor in an electrophotographic charging environment," J. Imaging Sci. Technol. **54**, 050304 (2010).

[14] D. S. Weiss, "Surface injection in corona-charged molecularly doped polymer films," J. Imaging Sci. Technol. **34**, 132–135 (1990).